Noname manuscript No.
(will be inserted by the editor)

Weighing the antiproton

precision laser spectroscopy of antiprotonic helium atoms

Ryugo S. Hayano

Received: date / Accepted: date

Abstract Antiprotonic helium is a metastable three-body neutral atom consisting of an antiproton, a helium nucleus and an electron, which we serendipitously discovered some 20 years ago. The antiproton, which normally annihilates within a few picoseconds when injected into matter, can be "stored" in this system for up to several microseconds, and laser spectroscopy is possible within this time window. From the laser transition frequency, the antiproton-to-electron mass ratio can be deduced to high precision. Recent progress at CERN's antiproton decelerator (AD) will be discussed.

Keywords CODATA · Antiprotonic atom · Laser spectroscopy

1 Introduction

It was in late 80's at the 12-GeV proton synchrotron at KEK, Japan, when we found an intriguing effect of $\bar{p}$ longevity in helium[1]. In the $\bar{p}$ annihilation time spectrum shown in Fig. 1, the peak at $t = 0$ is due to the normal, prompt annihilation. This however is followed by an anomalous delayed component, indicating that about 3% of antiprotons trapped in liquid helium survive with a mean lifetime of 3 μs. This was the beginning of our long series of experiments on antiprotonic helium.

Supported by MEXT grant 20002003 (Japan).

R.S. Hayano
Department of Physics, The University of Tokyo
7-3-1 Hongo, Bunkyo-ku, Tokyo 113-0033, Japan
Tel.: +81-3-5841-4235
E-mail: hayano@phys.s.u-tokyo.ac.jp

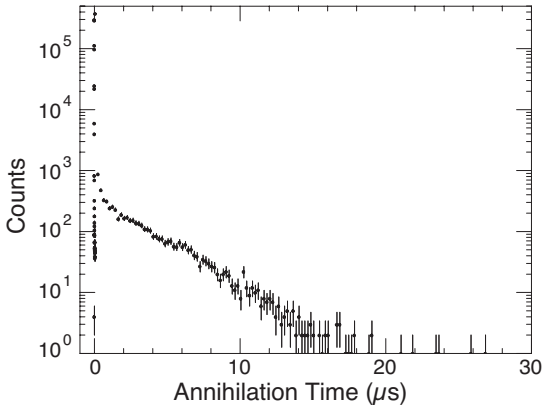

Fig. 1 The antiproton annihilation time spectrum measured by stopping antiprotons in liquid helium at KEK. From [1].

2 Metastability of antiprotonic helium

This anomalous longevity is now ascribed to the formation of the antiprotonic helium atoms (hereafter denoted $\bar{p}\mathrm{He}^+$), which have the following remarkable features:
1. The metastability occurs when the antiproton occupies a near-circular orbit having a large $n(\sim 38)$ and also large $\ell(> 35)$.
2. We usually use low-temperature ($T \sim 10$ K) helium gas as the target. The $\bar{p}^4\mathrm{He}^+$ atoms that are produced collide with the surrounding helium atoms and are thermalized, without being destroyed. Therefore, the antiprotonic helium atoms are already cold and are well suited for high-precision spectroscopy.

Figure 2 shows an energy level diagram of $\bar{p}^4\mathrm{He}^+$. The levels indicated by the continuous lines have metastable ($> 1\mu$s) lifetimes and de-excite radiatively, while the levels shown by wavy lines are short lived (< 10 ns) and de-excite by Auger transitions to antiprotonic helium ion states (shown by dotted lines). Since the ionic states are hydrogenic, Stark collisions quickly induce antiproton annihilation on the helium nucleus, also indicated in Fig. 2.

3 Principle of $\bar{p}\mathrm{He}^+$ Laser Spectroscopy

Laser spectroscopy of $\bar{p}\mathrm{He}^+$ works as follows: As shown in Fig. 2, there is a boundary between metastable states and short-lived states. For example, $(n, \ell) = (35, 33)$ is metastable, while $(n, \ell) = (34, 32)$ is short lived. Thus, if we use a laser to induce a transition from (35,33) to (34,32), (and of course if an antiproton happens to be occupying the (35,33) level at the time of laser ignition), the antiproton is deexcited to the short-lived state, which then Auger decays to an ionic $(n_i, \ell_i) = (30, 29)$ state within < 10 ns. The ionic state is then promptly destroyed by Stark collisions, leading to the nuclear absorption or annihilation of the antiproton. As a result, we can observe a sharp increase

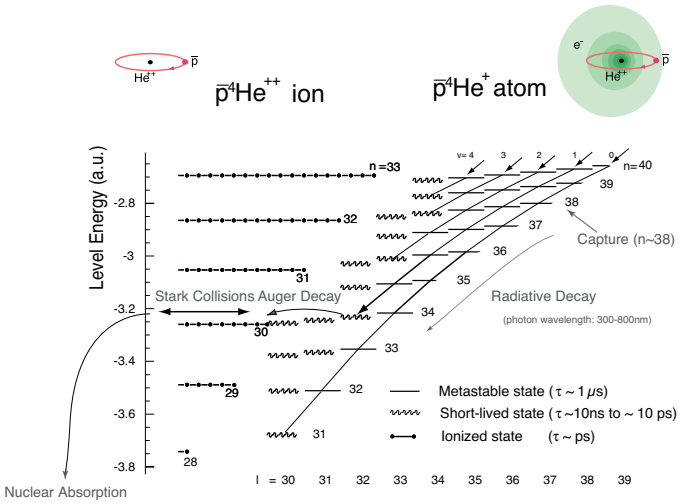

Fig. 2 The level diagram of $\bar{p}^4\mathrm{He}^+$ in relation to that of $\bar{p}^4\mathrm{He}^{++}$. The continuous and wavy bars stand for metastable and short-lived states, respectively, and the dotted lines are for $\ell-$degenerate ionized states.

in the $\bar{p}$ annihilation rate in coincidence with a resonant laser pulse, as shown in Fig. 3 [2]. We measure the intensity of the laser-induced annihilation spike as a function of laser detuning to obtain the transition frequency ν_{exp}. By comparing ν_{exp} with ν_{th} calculated by three-body QED theories [3–5], we can deduce $m_{\bar{p}}/m_e$.

4 Progress over the years

Fig. 4 compares the progress of experiment and theory over the years [6]. At LEAR (left-most points), we reached a precision of $\delta\nu/\nu$ of $0.5-1\times10^{-6}$ [7]. In our first experiment at the CERN AD, we measured six transition frequencies of $\bar{p}^4\mathrm{He}^+$ to $\delta\nu/\nu = 1 - 10 \times 10^{-7}$ [8]. The essential difference between the LEAR and the AD experiments is the time structure of the antiproton beam. At LEAR, antiprotons were slowly extracted from the LEAR ring, so that laser was fired for each $\bar{p}^4\mathrm{He}^+$-candidate event which occurred randomly with a mean rate of some 300Hz. In contrast, the AD provides a short pulse of $\sim$ 100-ns wide containing some $3 \times 10^7 \bar{p}$s, repeated every $\sim$ 100s. A single laser pulse in this case irradiates some 10^6 metastable atoms. The conventional event-by-event collection of antiproton-annihilation events used at LEAR is impossible with the pulsed beam at AD. We thus developed a new detection scheme based on analogue waveform recording of Čerenkov detectors viewed by gateable photomultipliers.

In the second series at AD, in 2003, we determined 7 transition frequencies of $\bar{p}^4\mathrm{He}^+$ and 6 of $\bar{p}^3\mathrm{He}^+$, with errors of $\delta\nu/\nu \sim 0.5 - 2 \times 10^{-7}$ [9]. This was made possible by constructing a radio-frequency quadrupole decelerator

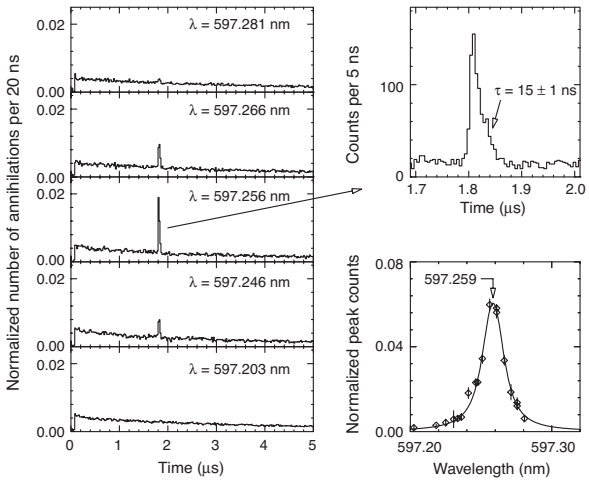

Fig. 3 Laser resonance of the $(39, 35) \rightarrow (38, 34)$ transition in $\bar{p}^4\mathrm{He}^+$. Left: Observed time spectra of delayed annihilation of antiprotons with laser irradiation of various wavelengths near 597.2nm. Upper right: Enlarged time profile of the resonance spike. Lower right: Normalized peak count versus wavelength in the resonance region. From [2]

.

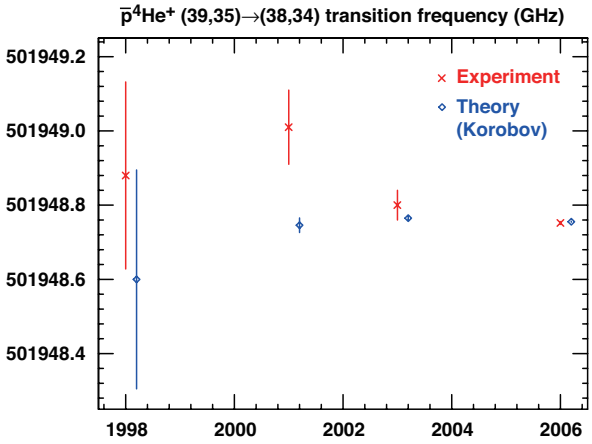

Fig. 4 Comparison of measured and calculated transition frequencies for the $(39, 35) \rightarrow (38, 34)$ transition of $\bar{p}^4\mathrm{He}$. From [6].

(RFQD), which decelerates the 5.3 MeV antiprotons ejected from the AD ring to < 100 keV with an efficiency of 20-25% [10], so that the antiprotons could be stopped in a much lower-density target having $\rho \sim 10^{17}$ cm^{-3}, removing the uncertainties due to collisional effects.

Having eliminated the collisional shift, the line width of the laser and its frequency calibration remained as the largest contributory factors to the errors on measured values of the resonant frequencies. Only pulsed lasers can provide

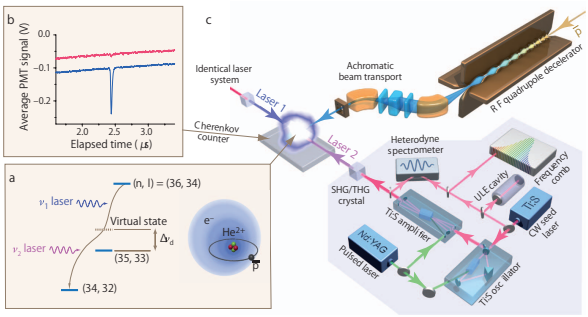

Fig. 5 (a) Energy level diagram involving the two-photon transition $(n, \ell) = (36, 34) \rightarrow (34, 32)$ of $\bar{p}^4\mathrm{He}^+$, (b) Cherenkov signal showing annihilation of $\bar{p}^4\mathrm{He}^+$ following this two-photon resonance induced at $t = 2.4\mu$s by two counterpropagating beams (solid blue line). Spectrum measured when one of the lasers is detuned -500 MHz away from resonance condition (red), (c) Experimental layout. From Ref. [13].

the megawatt-scale intensities needed here to induce the $\bar{p}\mathrm{He}^+$ transitions. However, fluctuations in their frequency and line width and the difficulty of calibrating the wide range of $\bar{p}\mathrm{He}^+$ wavelengths (from infrared to ultraviolet) have limited our experimental precision. We circumvented these problems by basing our experiments on a continuous-wave (cw) laser whose frequency ν_{cw} could be stabilized with a precision $< 4 \times 10^{-10}$ against an optical comb. Its intensity was then amplified by a factor 10^6 to produce a pulsed laser beam of frequency $\nu_{\mathrm{pl}} \sim \nu_{\mathrm{cw}}$ with an accuracy and resolution $1-2$ orders of magnitude higher than before. This made it possible for us [11] to reach the precision indicated by the right-most point in Fig. 4.

5 Weighing the antiproton

The ν_{exp} values thus obtained were compared with theoretical values ν_{th} [4,5], which included QED and nuclear-size ($\Delta_{\mathrm{nuc}} = 2 - 4$ MHz) effects, and used the 2002 CODATA recommended values for fundamental constants. Theory also provided coefficients for $d\nu_{\mathrm{th}}/d(m_p/m_e)$. These we used to determine the antiproton-to-electron mass ratio, by minimizing the sum $\Sigma[\nu_{\mathrm{th}}(m_{\bar{p}}/m_e) - \nu_{\mathrm{exp}}]^2/\sigma^2_{\mathrm{exp}}$ over the 12 transitions, to be 1,836.152674(5) [11]. This result was included in the evaluation of the CODATA 2006 fundamental physical constants [12].

Recently, we succeeded to achieve a higher frequency precision by performing a two-photon resonance (by using two counter-propagating beams, as shown in Fig. 5), which canceled the first order Doppler width, and determined $m_{\bar{p}}/m_e$ to be 1,836.1526736(23) [13]. This result, compared with the proton-to-electron mass ratios measured in previous experiments in Fig. 6 was included in the evaluation of the CODATA 2010 fundamental physical constants [19].

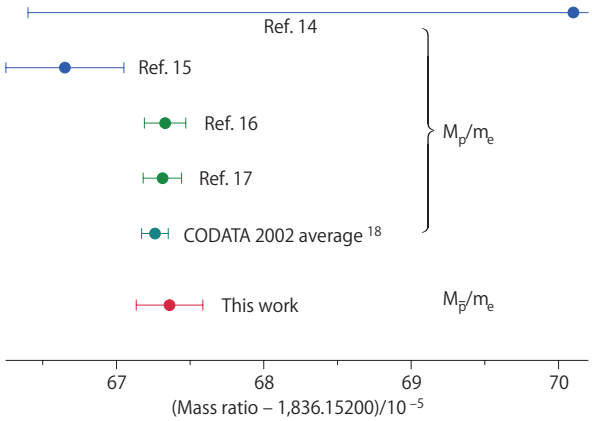

Fig. 6 Proton-to-electron mass ratios measured in previous experiments [14–17] and the CODATA 2002 recommended value obtained by averaging them [18], compared with the antiproton-to-electron mass ratio measured by the present work. From Ref. [13].

Acknowledgements I would like to thank our collaborators in the CERN ASACUSA collaboration, Drs. M. Hori, E. Widmann and D. Horvath in particular, and the staff at the CERN AD for much help and support. This work was supported by MEXT grant 20002003 (Japan).

References

1. M. Iwasaki et al., Phys. Rev. Lett. **67**, 1246 (1991).
2. N. Morita et al.: Phys. Rev. Lett. **72**, 1180 (1994).
3. V. I. Korobov, in Proceedings of EXA05, (Austrian Academy of Sciences Press, Vienna, 2005).
4. V. I. Korobov, Phys. Rev. A 73, 022509 (2006).
5. V. I. Korobov (private communication, 2007).
6. R.S. Hayano et al., Reports on Progress in Physics **70**, 1995 (2007).
7. H.A. Torii et al.: Phys. Rev. A **59**, 223 (1999).
8. M. Hori et al.: Phys. Rev. Lett. **87**, 093401 (2001).
9. M. Hori et al.: Phys. Rev. Lett. **91**, 123401 (2003).
10. A.M. Lombardi et al., in Proceedings of the 2001 Particle Accelerator Conference , Chicago, 2001 (IEEE, Piscataway, NJ, 2001), pp. 585.
11. M. Hori et al., Phys. Rev. Lett. **96**, 243401 (2006).
12. P. J. Mohr and B. N. Taylor, Rev. Mod. Phys. **80**, 633 (2008).
13. M. Hori, et al., Nature **475**, 484 (2011).
14. R.S. Van Dyck Jr, F.L. Moore, D.L. Farnham, P.B. Schwinberg, Bull. Am. Phys. Soc. **31**, 244 (1986).
15. D.L. Farnham, R.S. Van Dyck Jr., P.B. Schwinberg, Phys. Rev. Lett. **75**, 3598 (1995).
16. T. Beier, et al., Phys. Rev. Lett. **88**, 011603 (2002).
17. J. Verdú, et al., Phys. Rev. Lett. **92**, 093002 (2004).
18. P.J. Mohr, B.N. Taylor, Rev. Mod. Phys. **77**, 1 (2005).
19. `http://physics.nist.gov/cuu/Constants/`